Synthesis, Characterization, and Magnetic Properties of Uniform-sized MnO Nanospheres and Nanorods

Jongnam Park,[†] Eunae Kang,[†] Che Jin Bae,[‡] Je-Geun Park,[‡] Han-Jin Noh,[§] Jae-Young Kim,[§] Jae-Hoon Park,[§] Hyun Min Park,[||] and Taeghwan Hyeon*,[†]

National Creative Research Initiative Center for Oxide Nanocrystalline Materials and School of Chemical Engineering, Seoul National University, Seoul 151-744, Korea, Department of Physics and Institute of Basic Sciences, Sungkyunkwan University, Suwon 440-746 Korea, Department of Physics and Pohang Acceleration Laboratory, Pohang University of Science and Technology, Pohang, Kyungbuk 790-784, Korea, and New Material Evaluation Center, Korea Research Institute of Standards and Science, Taejon 305-600, Korea

Received: April 22, 2004; In Final Form: July 5, 2004

Uniform-sized MnO nanospheres and nanorods were fabricated by the thermal decomposition of Mn−surfactant complexes. The particle sizes of the nanospheres were varied from 5 to 40 nm by changing the surfactant. The shape of the particles could be controlled by varying the experimental conditions. The synthesized MnO nanorods have diameters ranging from 7 to 10 nm, and lengths ranging from 30 to 140 nm. Structural characterization using X-ray powder diffraction, X-ray absorption spectroscopy, and high-resolution transmission electron microscopy revealed that the nanoparticles are core/shell structures with a MnO core and a thin Mn_3O_4 shell. The MnO nanoparticles exhibited very interesting magnetic properties. For example, the MnO nanorods with dimensions of 7 nm × 33 nm showed two blocking temperatures at 35 and 280 K, respectively.

The development of nanoparticles has been intensively pursued, not only for their fundamental scientific interest, but also for many technological applications.[1] For many of these applications, the synthesis of uniform-sized nanoparticles is of key importance, because the electrical, optical, and magnetic properties of these nanoparticles depend strongly on their dimension. For example, uniform-sized magnetic nanoparticles have attracted a lot of attention because of their broad range of applications, which include magnetic storage media, ferrofluids, magnetic resonance imaging (MRI), and magnetically guided drug delivery.[2] Recently, one-dimensional (1-D) nanostructured materials, including nanorods, nanowires, and nanotubes, have received a tremendous amount of attention because of their unique properties. These properties are derived from their low dimensionality, and their potential use in the interconnects and functional blocks that are used for fabricating nanoscale devices.[3] Manganese oxides have found wide applications as catalysts and electrode materials.[4] Very recently, several groups reported the synthesis of nanoparticles of manganese oxides.[5] Very interestingly, these MnO nanoparticles exhibited ferromagnetic characteristics, even though this material is antiferromagnetic in the bulk form. Herein, we report on the synthesis of MnO nanospheres and nanorods from the thermal decomposition of Mn−surfactant complexes. To the best of our knowledge, this is the first report on the synthesis of anisotropic manganese oxide nanoparticles.

The synthetic procedure reported herein is a modified version of a method that was used by our group for the synthesis of monodisperse nanocrystals of metals, metal oxides, and metal sulfides, and which employs the formation of a metal−surfactant complexes followed by aging at high temperature.[6] In the typical synthesis, a stock solution of Mn−surfactant complex, prepared by reacting 0.2 g of $Mn_2(CO)_{10}$ with 2 mL of oleylamine at 100 °C, was rapidly injected into 10 mL of trioctylphosphine (TOP) under vigorous stirring at 300 °C. The reaction temperature was then decreased to 280 °C and the resulting solution was stirred at this temperature for 1 h. The initial scarlet color of the solution slowly turned brownish black, indicating that nanoparticles were generated. The reaction mixture was then cooled to room temperature and the nanoparticles were retrieved by adding 50 mL of anhydrous ethanol, followed by centrifugation. The retrieved powder form of the nanoparticles could be easily redispersed in nonpolar organic solvents such as hexane or toluene.

The nanoparticles were characterized by transmission electron microscopy (TEM), powder X-ray diffraction (XRD), X-ray absorption spectroscopy (XAS), magnetic circular dichroism (MCD), and by means of a superconducting quantum interference device (SQUID). Figure 1a shows a TEM image of the 5-nm MnO nanoparticles, demonstrating the uniformity of the particles. This high-resolution TEM (HRTEM) image of a nanoparticle revealed the highly crystalline nature of the nanoparticles. The diameters of the MnO nanoparticles could be controlled by varying the phosphines that were used both as solvents and as stabilizing agents. When triphenylphosphine was employed in the synthesis instead of TOP, 10-nm MnO nanoparticles were produced (Figure 1b). The HRTEM image of a single 10-nm MnO nanoparticle showed that the nanoparticles were highly crystalline. When the reaction mixture prepared in TOP was aged at 100 °C for 2 days, 40-nm monodisperse MnO nanoparticles were produced (Figure 1c). Very similar results were reported by O'Brien et al.[5b] These monodisperse nanoparticles were obtained without going through any size selection process, which is a very important requirement for large-scale production.

* thyeon@plaza.snu.ac.kr.
[†] Seoul National University.
[‡] Sungkyunkwan University.
[§] Pohang University of Science and Technology.
[||] Korea Research Institute of Standards and Science.

10.1021/jp048229e CCC: $27.50
Published on Web 08/14/2004

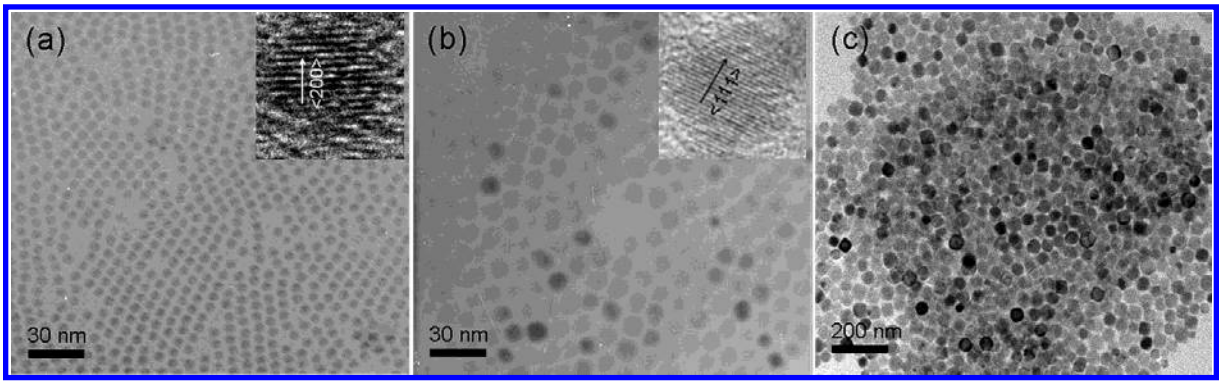

Figure 1. Transmission electron micrograph of 5-, 10-, and 40-nm monodisperse MnO nanoparticles.

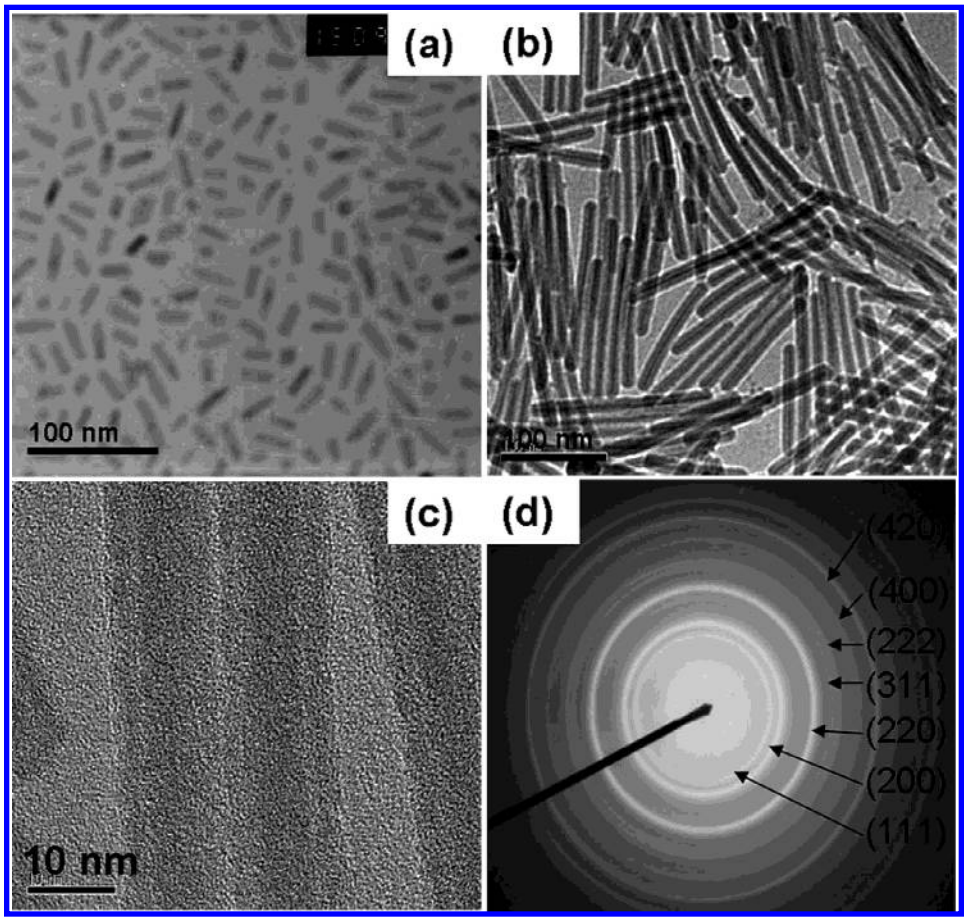

Figure 2. Low-resolution transmission electron micrographs of (a) 7 × 33 nm and (b) 8 × 140 nm sized MnO nanorods, (c) high-resolution transmission electron micrograph, and (d) electron diffraction pattern of 8 × 140 nm sized MnO nanorods.

The shape of the MnO nanoparticles could easily be controlled by changing the reaction temperature. It is known that one-dimensional nanorods are formed when two surfactants with different stabilizing capabilities are used under kinetically controlled conditions, such as those involving rapid thermal decomposition at high reaction temperature, whereas spherical nanoparticles are generated under thermodynamically controlled conditions, such as those involving the slow decomposition of the precursors and a long reaction time.[3] When the Mn−surfactant complex was injected rapidly into a TOP solution at 330 °C, rod-shaped MnO nanoparticles were predominantly produced (see the TEM image in the Supporting Information). Pure nanorods were obtained by a size-selection process that involved the addition of ethanol to a toluene solution containing a mixture of nanorods and nanospheres. The diameters and lengths of the nanorods were varied by using different phosphines. For example, when TOP and TPP were employed as the surfactants, MnO nanorods with dimensions of 7 nm (diameter) × 33 nm (length) and 8 nm (diameter) × 140 nm (length) were predominantly synthesized, respectively (Figures 2a and 2b). The crystal structure of the MnO nanorods was characterized using X-ray powder diffraction (XRD), electron diffraction (ED), and high-resolution TEM (HRTEM). The electron diffraction pattern of the TPP-stabilized nanorods with average dimensions of 8 nm × 140 nm, shown in Figure 2d, exhibited clear ring patterns demonstrating their polycrystalline nature. These ring patterns were assigned to the (111), (200), (220), (311), (222), (400), and (420) reflections of the face centered cubic (*fcc*) MnO structure (JCPDS # 07-0230). A high-resolution TEM image of the nanorods clearly revealed that they are polycrystalline materials composed of catenated spheres (Figure 3a). Consequently, the MnO nanorods seem to be synthesized by the aggregation of spherical nanoparticles through the cooperative interaction of two surfactants with

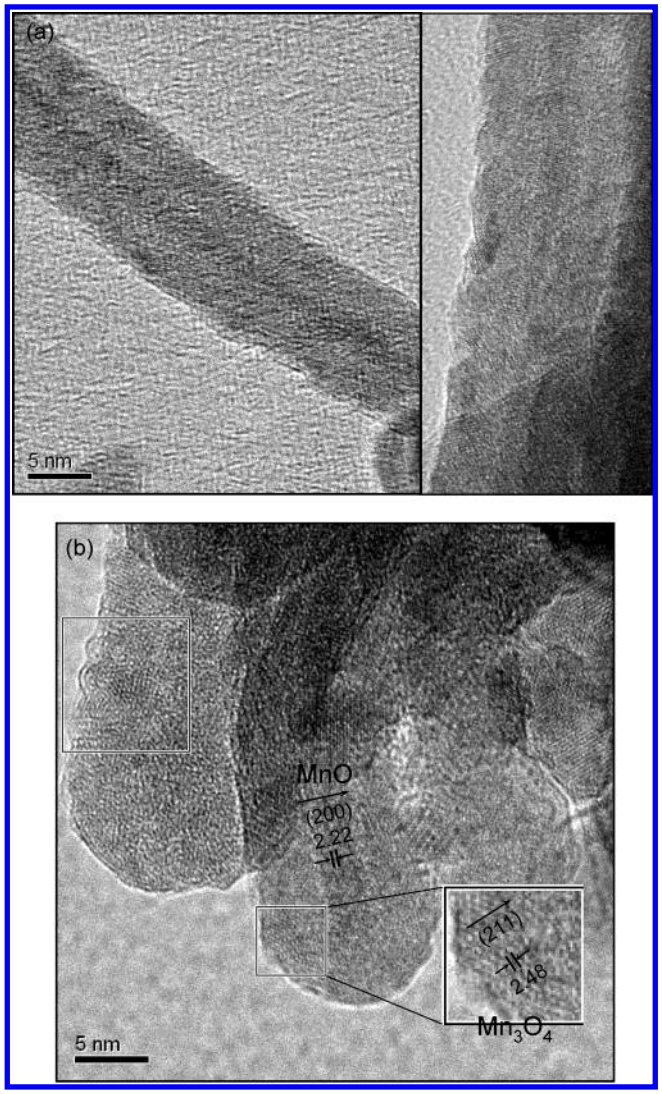

Figure 3. (a) High-resolution TEM (HRTEM) image of an 8 nm × 140 nm MnO nanorod showing its polycrystalline nature. (b) HRTEM image of an 8 nm × 140 nm MnO nanorod showing its core/shell structure.

different stabilizing capabilities under a kinetically controlled high-temperature condition. These structural characterizations revealed that the nanorods exhibit a core/shell structure with a MnO core and a thin Mn_3O_4 shell, as shown in the HRTEM image (Figures 2c and 3b). The XRD pattern of the nanorods showed that the nanorods were predominantly composed of *fcc* MnO and that a very small fraction of the Mn_3O_4 phase was also present (Figure 4).

To identify the oxidation state of Mn, X-ray absorption spectroscopy (XAS) measurements at the Mn $L_{2,3}$-edges were carried out for the 5-nm MnO nanospheres at the Dragon beamline of the National Synchrotron Radiation Research Center (NSRRC) in Taiwan. The presence of different valence states of Mn would be expected to reveal itself in the form of different absorption energies and spectral line shapes.[7] Figure 5a shows the Mn $L_{2,3}$-edge XAS spectrum obtained from the 5-nm MnO nanospheres. This spectrum is dominated by the large 2*p* core−hole spin−orbit coupling energy, which divides them into the L_3 and L_2 regions at low and high photon energies, respectively. The spectrum displays a rather complicated line shape, indicating the presence of a mixture of different ionic states. Indeed, the observed spectral line shape could be reproduced by mixing the absorption spectra of the Mn^{2+} and Mn^{3+} oxidation states

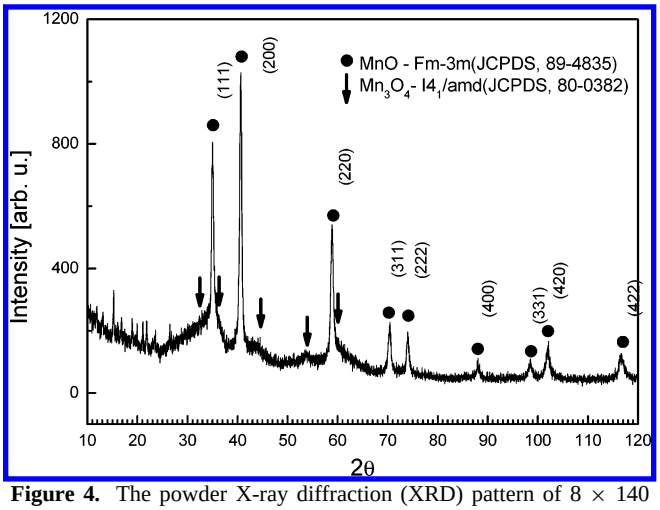

Figure 4. The powder X-ray diffraction (XRD) pattern of 8 × 140 nm sized MnO nanorods.

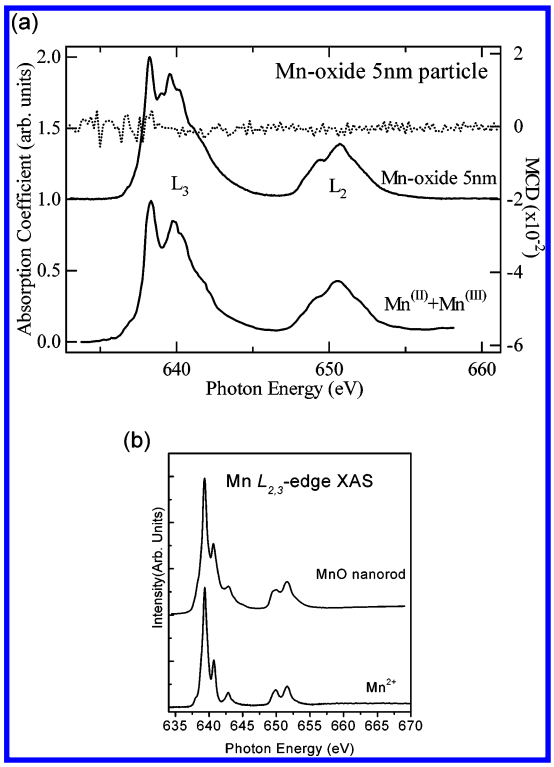

Figure 5. (a) Mn $L_{2,3}$-edge XAS spectrum of 5-nm MnO nanospheres compared with a 1:1 mixture of the spectra of Mn^{2+}(II) and Mn^{3+}(III) oxidation states. The corresponding MCD spectrum (dotted line) collected at 100 K is also presented. The spectra were obtained at the Dragon beamline of the National Synchrotron Radiation Research Center (NSRRC) in Taiwan. (b) Mn $L_{2,3}$-edge XAS spectrum of 7 nm × 33 nm MnO nanorods compared with a spectrum of the Mn^{2+}(II) oxidation state. The spectra were obtained at the EPU6 beamline of Pohang Light Source, Korea.

at a ratio of 1:1.[7] This result shows that the Mn-oxide state of the nanoparticles is not MnO, but a mixture of MnO and Mn_3O_4. X-ray magnetic circular dichroism (MCD) measurements using circularly polarized light were also performed, to test for the possibility of ferromagnetic ordering. As shown in Figure 5, there is no observable MCD signal, indicating that the nanoparticles have no significant ferromagnetic ordering at 100 K. We also conducted XAS studies of the MnO nanorods with dimensions of 7 nm × 33 nm at EPU6 beamline of Pohang Light Source. The oxidation state of Mn in nanorods is well proven by the XAS measurement to be nearly Mn^{2+}. The spectrum of Figure 5b is the Mn $L_{2,3}$-edge XAS spectrum

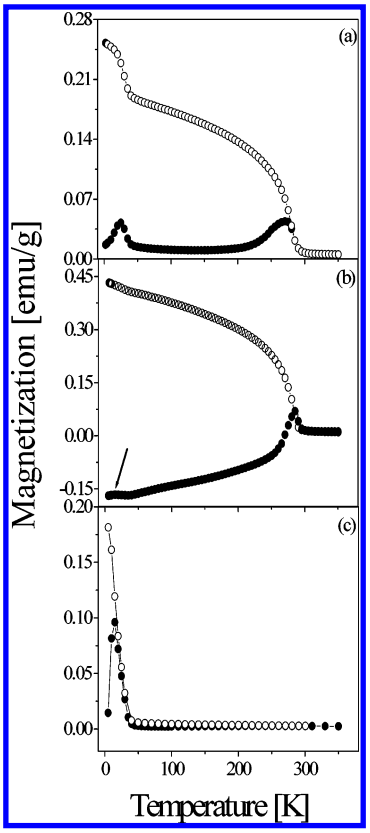

Figure 6. Temperature dependence of magnetization measured with applied field of 100 Oe for (a) MnO nanorods with 7 nm × 33 nm, (b) MnO nanorods with 8 nm × 140 nm, and (c) Mn_3O_4 nanospheres of 5 nm after zero-field cooling (solid symbols) and field cooling (open symbols). The arrow in the middle figure indicates the temperature at which the magnetization exhibits a small anomaly at low temperature.

obtained from the MnO nanorods and the spectrum of the Mn^{2+} ionic state. The similarity between them confirms that the nanorod is largely composed of MnO. The spectral deviation from that of Mn^{2+} in the high-energy side of both edges indicates the existence of a higher valence state such as Mn^{3+}. However, the relative amount of manganese ions with higher valence is very small.

We investigated the magnetic properties of several nanospheres and nanorods of MnO (nanospheres with diameters of 5 and 10 nm; nanorods with dimensions of 7 nm × 33 nm, 8 nm × 140 nm, and 5 nm × 300 nm) using a commercial superconducting quantum interference device (SQUID) magnetometer (Quantum Design, MPMS5XL), which is equipped with a 5 T superconducting magnet. All of our magnetization measurements were made from 2 to 360 K, after zero-field cooling (ZFC) or field cooling (FC), with an applied field of 100 Oe from 360 K. We also measured full hysteresis curves for all the samples up to 5 T. For comparative purposes, we also measured a 5-nm sphere of Mn_3O_4 that was prepared by an oxidation process with trimethylamine *N*-oxide. Moreover, several thin films of different MnO samples were also measured under the same conditions.

In Figure 6, typical magnetization curves are shown for three different samples: (a) MnO nanorods with dimensions of 7 nm × 33 nm, (b) MnO nanorods with dimensions of 8 nm × 140 nm, and (c) Mn_3O_4 nanospheres with a diameter of 5 nm. As can be seen in Figure 6a, the magnetization data of the MnO nanorods with dimensions of 7 nm × 33 nm exhibits a blocking temperature at around 280 K, at the point where the ZFC and FC curves begin to deviate from one another. Upon further

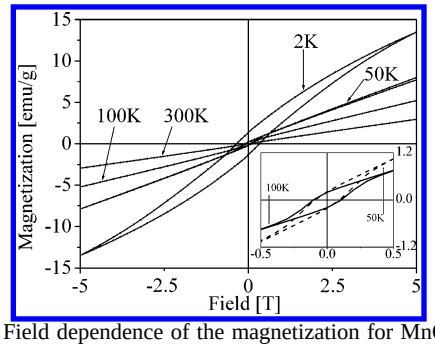

Figure 7. Field dependence of the magnetization for MnO nanorods with 7 nm × 33 nm measured after zero-field cooling from 360 K. The inset shows an enlarged figure for the magnetization data measured at 50 and 100 K.

cooling, there exists another anomaly below 35 K in both the ZFC and FC data. To understand the origin of these two anomalies, we prepared several MnO and Mn_3O_4 samples, as described above. As shown in Figure 6b, the second anomaly is considerably reduced for the other samples, although it is still visible at the same temperature in an enlarged figure. However, it is noticeable that the higher of the two blocking temperatures in Figure 6b appears at about the same temperature as that observed in Figure 6a. On the other hand, this higher blocking temperature is absent in the magnetization data for the Mn_3O_4 nanospheres, as shown in Figure 6c, although the lower transition temperature is still visible.

In Figure 7, the field dependence of the magnetization for the MnO nanorods with dimensions of 7 nm × 33 nm is shown at several temperatures: 2, 50, 100, and 300 K. At 300 K, the magnetization does not show any hysteresis at all, but at 100 K, which is below the blocking temperature, it displays a small but clear hysteresis, with a coercive field of 1000 Oe. However, below the lower transition temperature it exhibits a much larger hysteresis curve with a coercive field of almost 3200 Oe being observed at 2 K.

As regards the origin of the lower-temperature anomaly in the magnetization curve, we note that bulk Mn_3O_4 is known to have a ferrimagnetic transition at around 43 K, with a magnetic anisotropy constant of 1.6×10^6 erg/cm^3.[8] There has also been a very recent report[5c] that indicated that nanoparticles of Mn_3O_4 with sizes ranging from 6 to 15 nm show an anomaly in their magnetization below 40 K, which is very similar to our data. Therefore, we ascribe the lower-temperature anomaly to the blocking temperature of Mn_3O_4. In fact, our estimation of the magnetic anisotropy for the 5-nm Mn_3O_4 sphere is about 8×10^5 erg/cm^3, which is not far from the corresponding value for bulk Mn_3O_4. However, the origin of the higher-temperature anomaly is much more elusive and difficult to understand. We emphasize that the higher-temperature anomaly was observed without exception in all eight samples having different sizes and shapes, although the actual temperature of the anomaly varied depending on the size and shape of each sample. Therefore, we have no doubt that the higher-temperature transition is an intrinsic property of the samples. According to our microscopic measurements using X-ray diffraction and X-ray absorption spectroscopy (described above), we found that all of the MnO samples showed the presence of an Mn_3O_4 phase, even though they were originally prepared with a nominal MnO composition. This, we think, indicates that our MnO samples have a shell structure consisting of a Mn_3O_4 phase. The presence of this Mn_3O_4 phase at the surface of the nanoparticles would explain why the magnetization data for all of the MnO samples show some indication, albeit significantly reduced in certain cases, of the lower-temperature transition, which we ascribed

to the presence of the Mn_3O_4 phase. This makes one wonder what the origin of the higher-temperature transition is. We acknowledge that all possible Mn oxides, including MnO or Mn_3O_4 at least in their bulk forms, do not have transitions anywhere near the higher-temperature anomaly. Although we do not have a clear explanation as to the reason for the high-temperature anomaly, we note that MnO is known to have very high Curie−Weiss temperature of 548 K,[9] which is much higher than its bulk transition temperature of 122 K.[10] This big discrepancy between the two temperatures of bulk MnO leads to the unusual observation that there is a strong diffusive mode above the Neel temperature in neutron diffraction experiments, indicating the presence of short-range magnetic correlations.[11] It may just be possible that at reduced dimensions the short-range magnetic correlations build up more effectively than those in bulk MnO, and that the nanoparticles of MnO might possibly have a transition temperature that is higher than the T_N of bulk MnO. At the same time, the antiferromagnetic state of bulk MnO may not be a true ground state of the MnO nanoparticles, because of their large surface-to-volume ratio. This may inevitably lead to there being a new stable magnetic state with ferromagnetic components for the nanosized MnO samples. This kind of finite effect has already been found to occur for NiO.[12] Another explanation, somewhat related to the one just given above, is the effect of surface spins. It may well be conceivable that Mn spins near the surface layers may order differently from Mn spins at the core of the nanoparticles due to broken bonding at the surface. This then can make some contribution, as we have observed. Nonetheless, we admit that this explanation needs further experimental confirmation.

In conclusion, we synthesized uniform-sized MnO nanospheres with particle sizes ranging from 5 to 40 nm from the thermal decomposition of Mn−surfactant complexes. When the Mn−surfactant complexes were injected rapidly into a hot surfactant solution, MnO nanorods were produced. The sizes of the nanorods could be varied by using different phosphines. When TOP and TPP were employed as the surfactants, MnO nanorods with sizes of 7 nm (diameter) × 33 nm (length) and 8 nm (diameter) × 140 nm (length) were produced, respectively. Detailed structural characterization using XRD and XAS showed that the nanorods have a core/shell structure with a thin Mn_3O_4 shell. The MnO nanorods with dimensions of 7 nm × 33 nm showed two blocking temperatures at 35 and 280 K, respectively.

Acknowledgment. T.H. would like to thank the National Creative Research Initiative program for the financial support. J.G.P. acknowledges the support of the Proton Accelerator User Program (No. M102KS010001-02K1901-01810) of Proton Engineering R & D Project of the Ministry of Science and Technology.

Supporting Information Available: Powder X-ray diffraction (XRD) pattern of 5-nm sized MnO nanospheres and the TEM image of MnO nanorods prepared using triphenylphosphine before the size selection process. This material is available free of charge via the Internet at http://pubs.acs.org.

References and Notes

(1) (a) *Nanoparticles: From Theory to Application*; Schmid, G., Ed.; Wiley-VCH: Weinheim, 2004. (b) *Nanoscale Materials in Chemistry*; Klabunde, K. J., Ed.; Wiley-Interscience: New York, 2001. (c) Sugimoto, T. *Monodispersed Particles*; Elsevier Science: Amsterdam, 2001. (d) Fendler, J. H. *Nanoparticles and Nanostructured Films*; Wiley-VCH: Weinheim, 1998. (e) Alivisatos, A. P. *Science* **1996**, *271*, 933. (f) Pacholski, C.; Kornowsli, A.; Weller, H. *Angew. Chem., Int. Ed.* **2002**, *41*, 1188.

(2) (a) Hyeon, T. *Chem. Comm.* **2003**, 927. (b) Sun, S.; Murray, C. B.; Weller, D.; Folks, L.; Moser, A. *Science* **2000**, *287*, 1989. (c) Redl, F. X.; Cho, K.-S.; Murray, C. B.; O'Brien, S. *Nature* **2003**, *423*, 968. (d) Dumestre, F.; Chaudret, B.; Amiens, C.; Renaud, P.; Fejes, P. *Science* **2004**, *303*, 821. (e) Jacobs, K.; Zaziski, D.; Scher, E. C.; Herhold, A. B.; Alivisatos, A. P. *Science* **2001**, *293*, 1803. (f) Michler, P.; Imamoglu, A.; Mason, M. D.; Carson, P. J.; Strouse, G. F.; Buratto, S. K. *Nature* **2000**, *406*, 968. (g) Sun, S.; Murray, C. B. *J. Appl. Phys.* **1999**, *85*, 4325. (h) Sun, S.; Zeng, H. *J. Am. Chem. Soc.* **2002**, *124*, 8204.

(3) (a) Xia, Y.; Yang, P.; Sun, Y.; Wu, Y.; Mayers, B.; Gates, B.; Yin, Y.; Kim, F.; Yan, H. *Adv. Mater.* **2003**, *15*, 353. (b) Special issue on nanowires, *Adv. Mater.* **2003**, *15*, 351. (c) Hu, J. T.; Odom, T. W.; Lieber, C. M. *Acc. Chem. Res.* **1999**, *32*, 435. (d) Park, S.-J.; Kim, S.; Lee, S.; Khim, Z. G.; Char, K.; Hyeon, T. *J. Am. Chem. Soc.* **2000**, *122*, 8581. (e) Dumestre, F.; Chaudret, B.; Amiens, C.; Respaud, M.; Fejes, P.; Renaud, P.; Zurcher, P. *Angew. Chem., Int. Ed.* **2003**, *42*, 5213. (f) Dumestre, F.; Chaudret, B.; Amiens, C.; Fromen, M.-C.; Casanove, M.-J.; Respaud, M.; Zurcher, P. *Angew. Chem., Int. Ed.* **2002**, *41*, 4286. (g) Park, J.; Koo, B.; Hwang, Y.; Bae, C.; An, K.; Park, J.-G.; Park, H. M.; Hyeon, T. *Angew. Chem., Int. Ed.* **2004**, *43*, 2282.

(4) (a) Kim, S. H.; Kim, S. J.; Oh, S. M. *Chem. Mater.* **1999**, *11*, 557. (b) Nayak, S. K.; Jena, P. *J. Am. Chem. Soc.* **1999**, *121*, 644. (c) Li, J.; Wang, Y. J.; Zou, B. S.; Wu, X. C.; Lin, J. G.; Guo, L.; Li, Q. S. *Appl. Phys. Lett.* **1997**, *70*, 3047. (d) Nardi, J. C. *J. Electrochem. Soc.* **1985**, *132*, 1787.

(5) (a) Lee, G. H.; Huh, S. H.; Jeong, J. W.; Choi, B. J.; Kim, S. H.; Ri, H.-C. *J. Am. Chem. Soc.* **2002**, *124*, 12094. (b) Yin, M.; O'Brien, S. *J. Am. Chem. Soc.* **2003**, *125*, 10180. (c) Seo, W. S.; Jo, H. H.; Lee, K.; Kim, B.; Oh, S. J.; Park, J. T. *Angew. Chem., Int. Ed.* **2004**, *43*, 1115.

(6) (a) Hyeon, T.; Lee, S. S.; Park, J.; Chung, Y.; Na, H. B. *J. Am. Chem. Soc.* **2001**, *123*, 12798. (b) Hyeon, T.; Chung, Y.; Park, J.; Lee, S. S.; Kim, Y.-W.; Park, B. H. *J. Phys. Chem. B* **2002**, *106*, 6831. (c) Kim, S.-W.; Park, J.; Jang, Y.; Chung, Y.; Hwang, S.; Hyeon, T.; Kim, Y. W. *Nano Lett.* **2003**, *3*, 1289. (d) Joo, J.; Yu, T.; Kim, Y.-W.; Park, H. M.; Wu, F.; Zhang, J. Z.; Hyeon, T. *J. Am. Chem. Soc.* **2003**, *125*, 6553.

(7) Cramer, S. P.; de Groot, F. M. F.; Ma, Y.; Chen, C. T.; Sette, F.; Kipke, C. A.; Eichhorn, D. M.; Chan, M. K.; Armstrong, W. H.; Libby, E.; Christou, G.; Brroker, S.; McKee, V.; Mullins, O. C.; Fuggle, J. C. *J. Am. Chem. Soc.* **1991**, *113*, 7937.

(8) Dwight, K.; Menyuk, N. *Phys. Rev. B* **1960**, *119*, 1470.

(9) Tyler, R. W. *Phys. Rev.* **1933**, *44*, 776.

(10) Roth, W. L. *Phys. Rev.* **1958**, *110*, 1333.

(11) (a) Shull, C. G.; Smart, J. S. *Phys. Rev.* **1949**, *76*, 1256. (b) Renninger, A.; Moss, S. C.; Averbach, B. L. *Phys. Rev.* **1966**, *147*, 418.

(12) Kodama, R. H.; Makhlouf, S. A.; Berkowitz, A. E. *Phys. Rev. Lett.* **1997**, *79*, 1393.